# Probing short-range gravity using quantum reflection

J. Bovnewicz

Department of Physics, The University of Texas at Austin, Austin, 78712, Texas, USA

C. A. Sackett

Department of Physics, University of Virginia, Charlottesville, Virginia 22904, USA (Dated: November 13, 2025)

Quantum reflection occurs when ultra-cold atoms are incident on a material surface with sufficiently low velocity. The reflecting matter wave can interfere with the incident wave to form a detectable pattern, and this pattern contains information about atom-surface interactions at micrometer scales. We discuss how such an interferometer could be used to probe for anomalous short-range forces that are predicted by some beyond-standard model theories. We compare a simple analytical model for the anomalous phase to numerical solution of both the linear and non-linear Schrödinger equations, finding good agreement. With interactions, the phase does depend on the atomic density, which can be a source of noise. We nonetheless predict that under realistic conditions, the reflection technique can reach sensitivities approaching those obtained with macroscopic objects, and significantly improve the limits on anomalous coupling to atoms.

### I. INTRODUCTION

Many models for physics beyond the standard model lead to predictions of new short-range forces near material objects [1, 2], including forces from axion [3-5] and chameleon [6, 7] fields. The significance of these predictions has motivated experimental tests, the most sensitive of which measure the force between two macroscopic objects [8-12]. However, measurements using microscopic objects like single atoms are also important, as some theories predict a suppression of the force on macroscopic objects. The suppression could arise from spin-dependent effects [13–15], as expected for axions, or from the chameleon field mechanism [16]. Experiments probing the force between neutral atoms and macroscopic objects have not revealed any anomalies [17–20], but comparatively little data is available about such forces at sub-mm length scales [21].

We propose here a method to search for gravity-like forces between a macroscopic object and an atom, based on the interference of matter waves produced by quantum reflection. Quantum reflection is a universal process that occurs when a sufficiently slow atom approaches a material surface [22–25]. If the de Broglie wavelength of the atom is large compared to the range of the attractive Casimir-Polder surface interaction, then the atom experiences the surface interaction as a sharp step from which it will reflect, much as an atom reflects from an attractive square-well potential in elementary quantum mechanics. Any novel force would be small compared to the electromagnetic Casimir-Polder force, so it would not have an appreciable effect on the reflection amplitude. Instead, we propose here to observe the quantum phase shift imparted to an atom during the reflection process. We show that this yields a sensitivity for individual atoms at nearly the same level achieved for macroscopic objects, down to length scales of a few micrometers.

A different method for probing atom-surface interactions was recently proposed by Bennett and O'Dell  $et\ al.$ 

[26], in which cold atoms are confined in an optical lattice near the surface. The force between the atom and the surface is probed by measuring the local Bloch oscillation frequency. Bloch oscillation frequencies have been measured with high precision for atoms in free space, but achieving similar precision for atoms very near a surface may be experimentally challenging.

Both the Bennett technique and the method proposed here rely on Casimir-Polder shielding to distinguish the small anomalous force from the large electromagnetic interaction. The shield consists of a thin layer of conducting material that is placed between the atom and a test mass whose surface is being probed. This suppresses the electromagnetic interaction with the test mass, so any changes produced by the test mass can be attributed to an anomalous force. Bennett and O'Dell provide a detailed calculation of this screening effect and show that a 50-nm thick gold layer is sufficient. To avoid spatial variations in the Casimir-Polder interaction, we consider a fixed conducting membrane in front of a movable test mass structure.

In Section II of this paper, we present a simple analytical approximation for the quantum reflection phase shift. In Section III, we develop a more realistic model based on numerical solution of the Schrödinger and Gross-Pitaevskii equations, and find that agreement with the analytical model is generally good. In Section IV, we discuss how an experimental measurement could be set up and estimate the sensitivity that could be achieved. Finally, Section V discusses possible extensions of the approach, along with a summary and conclusions.

### II. ANALYTICAL MODEL

We first consider an approximate analytical model for the quantum reflection process. The interaction between an alkali-metal atom and a surface can be described by the Casimir-Polder potential [27]

$$U(x) = -\frac{C_4}{(x+3\lambda_a/2\pi^2)x^3} \equiv -\frac{\hbar^2 \beta^2}{2m(x+3\lambda_a/2\pi^2)x^3}$$
(1)

where x is the distance to the surface,  $\lambda_a$  is the wavelength of the principle transition of the alkali, and  $C_4$  or  $\beta$  (with units of length) are alternative parameters to express the atom-surface interaction strength. For now, we consider  $x \gg \lambda_a$  and approximate  $U \propto x^{-4}$ .

Although quantum reflection is a distributed effect, the effect is strongest at the position where U(x) changes the most quickly relative to the local de Broglie wavelength of the particle [28, 29]. This position can be determined by maximizing the quantity

$$\left| \frac{1}{k(x)U} \frac{dU}{dx} \right|, \tag{2}$$

where k(x) is the local wave number

$$k(x) = \left[\frac{2m}{\hbar^2} \left(E_0 - U(x)\right)\right]^{1/2} \tag{3}$$

for a particle with incident energy  $E_0$ . Setting  $E_0 = \hbar^2 k_0^2/2m$  leads to

$$k(x) = \left(k_0^2 + \frac{\beta^2}{x^4}\right)^{1/2},$$
 (4)

and (2) is maximized at

$$x_0 = \left(\frac{\beta}{k_0}\right)^{1/2}. (5)$$

We interpret  $x_0$  as the point of closest approach for the reflecting particle in a semi-classical model.

The quantum reflection process is efficient only for incident velocities less than  $v_c = \hbar/(4m\beta)$ . However, high reflection is not strictly needed for a interferometric measurement, since the amplitude of the interference pattern will scale as the square root of the reflection probability. Pasquini *et al.* observed reflection probabilities above  $10^{-2}$  for incident velocities up to  $5v_c$  [24].

We are interested in how the phase of the reflected quantum wave changes in the presence of an anomalous short-ranged interaction. We suppose the interaction between point masses m and M separated by distance r to have the Yukawa form [30]

$$V(r) = -\frac{GMm}{r} \alpha e^{-r/\lambda},\tag{6}$$

where G is Newton's constant,  $\alpha$  sets the strength of the interaction relative to gravity, and  $\lambda$  sets the range. The potential can be integrated to determine the net interaction between a particle and an infinite half-plane with mass density  $\rho$ , yielding

$$V(x) = -2\pi G \rho m \alpha \lambda^2 e^{-x/\lambda}.$$
 (7)

To estimate the phase shift produced by the Yukawa interaction, we use the semiclassical result [31]

$$\phi = -\frac{1}{\hbar} \int V(x) \, dt,\tag{8}$$

where the integral is over the classical path taken by the particle in the Casimir-Polder potential. We assume that the particle is incident from infinity with speed  $v_0 = \hbar k_0/m$ , approaches to distance  $x_0$  from (5), and then reflects and returns to infinity. The exact classical motion cannot be expressed in closed form, but we observe that at position  $x_0$ , the local wave number is  $\sqrt{2}k_0$ , corresponding to classical velocity  $\sqrt{2}v_0$ . This is not very different from  $v_0$ , so we make the simple approximation that the particle moves at constant velocity throughout the reflection. Then in Eq. (8), we use  $dt = \pm dx/v_0$  to obtain

$$\phi = -\frac{2}{\hbar v_0} \int_{x_0}^{\infty} V(x) dx = \frac{4\pi G\rho m}{\hbar v_0} \alpha \lambda^3 e^{-x_0/\lambda}.$$
 (9)

Using the critical velocity parameter  $v_c$  and eliminating  $x_0 = (\hbar \beta / m v_0)^{1/2}$ , we find

$$\phi = \frac{4\pi G\rho m}{\hbar v_0} \alpha \lambda^3 \exp\left[-\frac{2\beta}{\lambda} \left(\frac{v_c}{v_0}\right)^{1/2}\right]. \tag{10}$$

Below we compare this result to a detailed numerical model and find it to be reasonably accurate.

Note that the model assumes that the quantum reflection occurs only from the Casimir-Polder potential. If the incident velocity is too low, then the Yukawa potential itself can play a role and alter the behavior. This is avoided if |(1/kV)dV/dx| < 1 for  $x > x_0$ , as in Eq. (2). For the Yukawa potential (7),  $|(1/V)dV/dx| = 1/\lambda$ , so we require  $k_0\lambda > 1$ . This sets a velocity limit

$$v_0 > \frac{\hbar}{m\lambda} = \frac{4\beta}{\lambda} v_c. \tag{11}$$

To be consistent with  $v_0 \lesssim v_c$  we require  $\lambda \gtrsim 4\beta$ , which limits the short-range behavior that can be probed.

Table I gives values of  $\beta$ ,  $v_c$  and  $\phi/\alpha$  for the alkali elements on a conducting surface. We see that the highest sensitivity is achieved with the heaviest species. However, the low  $v_c$  values are potentially challenging. The corresponding kinetic energies are 90 pK for Rb and 30 pK for Cs, both comparable to the lowest temperature experiments to date [34, 35]. We focus here on Rb due to its less stringent cooling requirement as well as its simpler process for condensate production.

Because of the low temperatures involved, it would be difficult to prepare an incident wave function with well-defined energies at this level. We therefore consider an alternative approach wherein the confining forces on a stationary trapped cloud are turned off and the cloud is allowed to expand into the surface. In this situation there is a spread of incident velocities, but the expansion velocity can be reasonably well-defined and can be calculated

Species	$\beta$ ( $\mu$ m)	$v_c \; (\mathrm{mm/s})$	$\phi/\alpha$
$^7{ m Li}$	0.25	9.3	$1.7 \times 10^{-9}$
$^{23}Na$	0.46	1.5	$1.7 \times 10^{-8}$
$^{41}\mathrm{K}$	0.87	0.44	$5.0 \times 10^{-8}$
$^{87}\mathrm{Rb}$	1.4	0.13	$2.1 \times 10^{-7}$
$^{133}\mathrm{Cs}$	1.9	0.06	$4.5 \times 10^{-7}$

TABLE I. Quantum reflection parameters for different alkali atoms from a gold surface. The  $\beta$  values for K, Rb, and Cs are derived from the experimental measurements of Shih and Parsegian [32]. The  $C_3$  values reported there are a factor of 3.5 lower than theoretical values for a perfect conductor that are reported in Ref. [33]. To obtain  $\beta$  values for Li and Na, the perfect-conductor values were scaled down by the same factor. The critical reflection velocity  $v_c = \hbar/4m\beta$  gives the largest incident velocity for which quantum reflection will be efficient. The phase sensitivity  $\phi/\alpha$  is evaluated at  $\lambda=10$  µm, using Eq. (10) with  $v_0/v_c=4\beta/\lambda$  and a material density  $\rho=1.9\times10^4$  kg/m<sup>3</sup>.

in a mean-field model. As seen in Section III, the numerical results for this case remain in general agreement with the analytical approximation.

#### III. NUMERICAL MODELING

Numerical modeling of quantum reflection is challenging because the short-range atom-surface interactions are complicated. One way to avoid dealing with this complexity is to introduce an absorbing boundary condition in front of the surface, but it can be difficult to ensure the boundary is perfectly absorbing [36]. Any spurious reflections can distort the desired quantum reflection process. The alternative approach we use here is to smoothly transition the attractive Casimir-Polder potential to a constant value and allow atoms to continue propagating toward negative x [37]. The resulting potential is

$$\bar{U}(x) = \begin{cases} -\frac{C_4}{(x+b)x^3} & (x > x_2) \\ U_0 + A(x-x_1)^2 & (x_1 < x < x_2) \\ U_0 & (x < x_1) \end{cases}$$
(12)

where  $x_1$  and  $x_2$  define the boundaries of a transition zone. We abbreviate  $b = 3\lambda_a/2\pi^2$ . The potential and its first derivatives are continuous if

$$A = \frac{C_4}{2} \frac{4x_2 + 3b}{x_2^4 (x_2 + b)^2 (x_2 - x_1)}$$
 (13)

and

$$U_0 = -\frac{C_4}{2} \frac{6x_2^2 + 5x_2b - 4x_2x_1 - 3x_1b}{x_2^4(x_2 + b)^2}.$$
 (14)

A similar modification is applied to the Yukawa potential to produce a modified perturbation  $\bar{V}(x)$ .

We require the outer edge of the transition zone,  $x_2$ , to be well below the quantum reflection point  $x_0$  of Eq. (5).

For Rb atoms with  $v \approx v_c$ , we have  $x_0 \approx 3~\mu\mathrm{m}$ . The transition zone width  $x_2-x_1$  must be sufficiently large to provide a smooth potential and avoid spurious reflections. However, using a very wide transition zone leads to a large value of  $|U_0|$  and a high atomic velocity in the  $x < x_1$  region, which then requires an impractically small grid spacing for the numerical solution. For the calculations presented here, we use  $x_1=0.45~\mu\mathrm{m}$  and  $x_2=0.5~\mu\mathrm{m}$ , giving  $U_0/C_4=-15~\mu\mathrm{m}^{-4}$ .

We first consider the case of non-interacting atoms incident from infinity with a well-defined velocity  $-v_0$ . A fraction of the atoms will reflect to form an interference pattern, while the remainder continue propagating towards  $x = -\infty$  with velocity  $v_t = -(v_0^2 - 2U_0/m)^{1/2}$ . Here we solve the time-independent Schrödinger equation

$$-\frac{\hbar^2}{2m}\frac{\partial^2 \psi}{\partial x^2} + \left[\bar{U}(x) + \bar{V}(x)\right]\psi = E_0\psi \tag{15}$$

with  $E_0 = mv_0^2/2$  and a grid spacing of 1 nm. Since we expect only a single wave for  $x \leq 0$ , we start the solution at x = 0 with  $\psi(0) = 1$  and  $\psi'(0) = -ik_t \equiv$  $-imv_t/\hbar$ . We integrate towards positive x to find the solution for x large enough that  $|\bar{U}(x)| \ll E_0$ . In this large-x region, we expect  $\psi(x)$  to be of the form  $Ae^{-ikx} + Be^{ikx}$ . The interference pattern then has the form  $|\psi|^2 = |A|^2 + |B|^2 + 2|A||B|\cos(2kx + \theta)$  where  $\theta$ is the phase difference between A and B. To evaluate  $\theta$ , we numerically find a location  $x_{\text{max}}$  of a maximum in  $|\psi|^2$ . We analytically evaluate  $k(x_{\text{max}})$  using (4), and then take  $\theta = -2kx_{\text{max}}$ , modulo  $2\pi$ . We compute the Yukawa phase  $\phi$  by subtracting the  $\theta$  phase calculated using the nearest maximum of the numerical solution for  $\alpha = 0$ . The solid points in Fig. 1 show the results, and agree quite well with Eq. (10) for velocities above the velocity limit from Eq. (11). Below the velocity limit, the phase difference drops below the model's prediction as the Yukawa potential itself contributes to the reflection process.

To model the alternative experiment in which a stationary atom cloud is allowed to expand into a surface, we solved the time-dependent problem. Here we allow for atomic interactions in the one-dimensional Gross-Pitaevskii (GP) equation [38],

$$i\hbar\frac{\partial\psi}{\partial t} = -\frac{\hbar^2}{2m}\frac{\partial^2\psi}{\partial x^2} + \left[\bar{U}(x) + \bar{V}(x)\right]\psi + g|\psi|^2\psi, \quad (16)$$

with

$$g = \frac{4\pi\hbar^2 a}{m}\sigma,\tag{17}$$

where a=5.05 nm is the three-dimensional scattering length and  $\sigma=N/A$  is the area particle density for N atoms in transverse area A. Pasquini et al. [25] found that a mean-field calculation yielded good agreement with observed reflection probabilities for their experiments at much stronger interactions than we consider, so we expect the model to be adequate here.

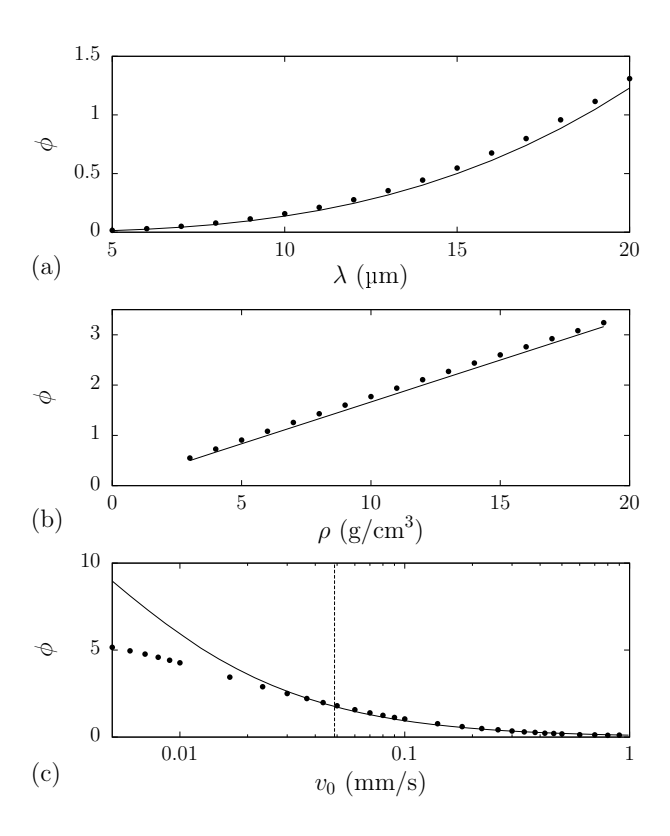


FIG. 1. Comparison between numerical results for a non-interacting gas (data points) and analytical model (curves). (a) The Yukawa perturbation phase  $\phi$  as a function of the Yukawa length  $\lambda$ , for <sup>87</sup>Rb atoms with incident speed  $v_0 = 0.2$  mm/s and a perturber density  $\rho = 3$  g/cm<sup>3</sup>. (b) Phase  $\phi$  vs. density  $\rho$ , for  $v_0 = 0.2$  mm/s and  $\lambda = 15$  µm. (c) Phase  $\phi$  vs. velocity  $v_0$ , for  $\lambda = 15$  µm and  $\rho = 3$  g/cm<sup>3</sup>. The vertical dashed line shows the velocity limit of Eq. (11). For all curves,  $\alpha = 10^7$ .

In our calculation, the initial wave function is first determined by solving the GP equation in imaginary time for atoms confined in a harmonic trap potential

$$V_{\text{trap}}(x) = \frac{1}{2}m\omega^2(x - x_t)^2,$$
 (18)

with  $\omega=2\pi\times0.5$  Hz and  $x_t=150~\mu\mathrm{m}$ . We then turn off the potential and allow the atoms to expand in real time towards the surface at x=0. We solve Eq. (16) using a Crank-Nicolson scheme with a grid spacing of 10 nm and a time step of 2.5  $\mu\mathrm{s}$  [39]. Figure 2 shows the atomic density distribution that results after an evolution time of 1.1 s, with and without the perturbation potential  $\bar{V}$ . The oscillations are the interference effect, and the phase shift from the perturbation is clear.

We again extract the Yukawa phase  $\phi$  by comparing the two interference patterns, with results shown at in Fig. 3. Here the data points correspond to different values of  $\alpha$  and  $\rho$ , with the phase normalized to the values used for the solid circles. As seen, the different results are compatible with each other when normalized this way.

The curve in Fig. 3 is the analytical result from

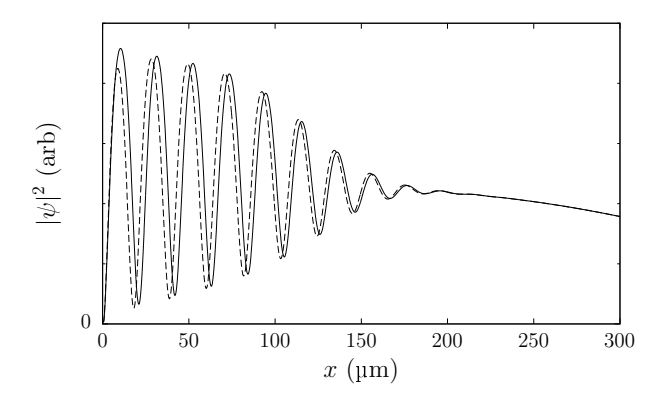


FIG. 2. Atom density distribution after quantum reflection from a gold surface. The oscillations are due to interference between the incident and reflected wave functions. The solid curve is obtained with only the Casimir-Polder surface interaction, while the dashed curved is obtained when including a Yukawa potential with  $\alpha=10^7$  and  $\lambda=15$  µm. Here we assume  $^{87}{\rm Rb}$  atoms with  $\sigma=10^{10}$  atoms/cm².

Eq. (10). However, in this configuration there is no definite incident velocity  $v_0$ . Instead, we estimate an effective  $v_0$  using the spatial period  $\Lambda$  of the interference fringe observed in the numerical solution at the position where the phase is measured. The pattern here is produced by atom waves with two different velocities  $v_{\rm inc}$  and  $v_{\rm ref}$ , where we expect  $|v_{\rm ref}| \gg |v_{\rm inc}|$ , since the reflected atoms have traveled considerably further than the incident atoms. For simplicity, we neglect  $v_{\rm inc}$  and set  $|v_{\rm ref}| = 2\pi\hbar/m\Lambda$ . We then use this velocity for  $v_0$  in Eq. (10). We find that  $\Lambda$  does depend slightly on the Yukawa perturbation, but again for simplicity, in Fig. 3 we use a fixed value of  $v_0$  determined from the interference pattern with no perturbation. As seen, this yields reasonably good agreement with the numerical solutions.

We also used the time-dependent model to investigate the effect of atomic interactions on the interference phase. Unsurprisingly, this effect is significant. Here we set the Yukawa interaction to zero and instead observe how the interference phase varies with the atom density  $\sigma$ . For the conditions of Fig. 2, we find that a 10% variation in  $\sigma$  leads to a phase shift of about 1 rad. This matters because in an experiment, the atom number typically fluctuates from run to run, making the interactions a source of phase noise. One way to mitigate this effect is to operate at a Feshbach resonance where interactions can be suppressed. Alternatively, the number of atoms can be determined with good accuracy at the same time that the interference pattern is observed. By comparing runs having similar number values, the impact of the Yukawa interaction could be extracted even in the presence of noise.

Two possible explanations for the atom-number sensitivity can be considered. First, the chemical potential of the initially-trapped atoms depends on  $\sigma$ , which in turn affects the expansion velocity of the released atoms and

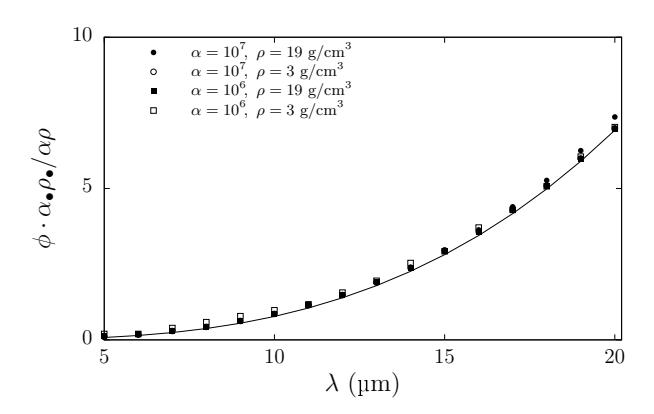


FIG. 3. Numerical and analytical results for an interacting <sup>87</sup>Rb gas reflecting from a gold surface. The Yukawa phase  $\phi$  is shown as a function of the interaction length  $\lambda$  for various values of interaction strength  $\alpha$  and surface density  $\rho$ , as indicated. To collapse the data to a uniform range, the phase values are scaled by  $1/\alpha\rho$ , relative to reference values  $\alpha_{\bullet} = 10^7$  and  $\rho_{\bullet} = 19$  g/cm<sup>3</sup>. Data points are numerical results from the Gross-Pitaevskii equation, and the curve is the analytical result of Eq. (10). The analytical formula was evaluated using  $v_0 = 0.225$  mm/s, obtained from the observed period of the interference pattern as seen in Fig. 2.

thus the reflection phase. Second, interactions that occur during the reflection process itself could modify the phase directly. To isolate these possibilities, we observe how the wavelength of the interference pattern varies with  $\sigma$ , and interpret that in terms of an effective velocity variation. We then use the non-interacting model to see how this velocity variation would affect the phase. We find that the interaction-induced velocity variation corresponds to a phase shift of only a few mrad, much smaller than observed in the model. We conclude that the phase sensitivity comes primarily from non-trivial interaction effects arising during the reflection process.

## IV. IMPLEMENTATION

We consider here practical aspects of the proposed measurements and estimate the sensitivity that could be achieved. We take the atomic source to be a Bose-Einstein condensate confined in trap that is positioned near the reflecting wall. For instance, an Ioffe-Pritchard magnetic trap could be aligned with its weak axis perpendicular to the wall. The parameters of Fig. 2 could be achieved using  $2 \times 10^4$  <sup>87</sup>Rb atoms in a harmonic trap with 5 Hz transverse oscillation frequency. We envision a Bose condensate being prepared in this potential, moved near to the wall, and then released by turning off the x confinement. Once the interference pattern is established, it can be observed using standard absorption imaging. To probe for short-range gravitational effects, it is necessary to vary the density of the reflecting test mass. It is critical to so without affecting the surface position, Casimir-Polder potential, or electrostatic

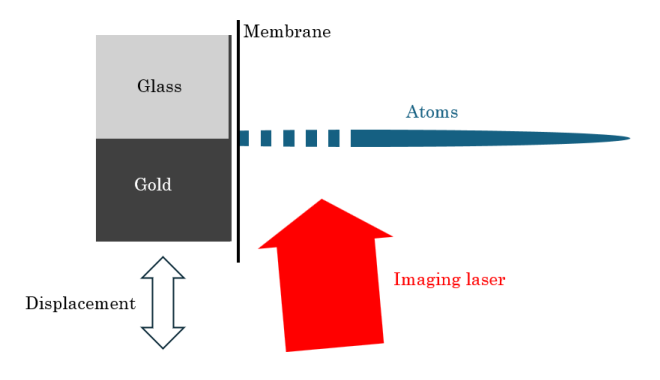


FIG. 4. (Color online) Schematic layout for quantum reflection interferometer. A Bose condensate (blue) in an elongated trap potential is allowed to expand into a conductive membrane. The membrane sits just in front of a test mass consisting of bonded gold and glass blocks. The test mass can be translated roughly 50 µm parallel to the surface to vary the density which which the atoms interact. An absorption imaging laser beam (red) passes through the atoms at a small angle, reflects from the membrane, and is then imaged by a camera (not shown). A secondary imaging system perpendicular to the plane of the drawing is used to locate the atoms relative to the boundary between test-mass sections.

patch potentials. An established way to achieve this is to screen the test mass with a thin conducting membrane [40]. The membrane thickness should be small compared to the Yukawa length  $\lambda$ , here 5 µm or larger. The membrane must also be thick enough to effectively screen the variable surface: Bennett et~al. have calculated that 50 nm is sufficient for a good conductor like gold. Suitable membrane materials include silicon nitride or beryllium, which can be as thin as a few nm and subsequently coated to the thickness desired [41, 42].

The test mass itself could be implemented as a uniform material whose position can be adjusted to be either near (distance small compared to  $\lambda$ ) or far (distance large compared to  $\lambda$ ) from the membrane. Alternatively, the test mass could be constructed by bonding two materials of low and high density, which is then moved parallel to the membrane in order to vary the density near the atoms. A potential advantage of the second technique is that any electrostatic coupling between the test mass and membrane would remain approximately constant, suppressing induced motion of the membrane. Suitable contrasting materials include gold ( $\rho = 19 \text{ g/cm}^3$ ) and glass  $(\rho = 3 \text{ g/cm}^3)$ . A thin coating of gold over the glass material would further stabilize coupling to the membrane by presenting a uniform surface. Figure 4 illustrates a possible configuration for this approach.

For imaging, a resonant laser beam can pass through the atoms, parallel to the membrane. With a fringe spacing of around 20  $\mu$ m, high spatial resolution is not required. However, imaging atoms near a surface can be challenging due to diffraction from the surface edge. One solution is to take advantage fact that the fringe spacing is comparable to the approximately 10  $\mu$ m transverse

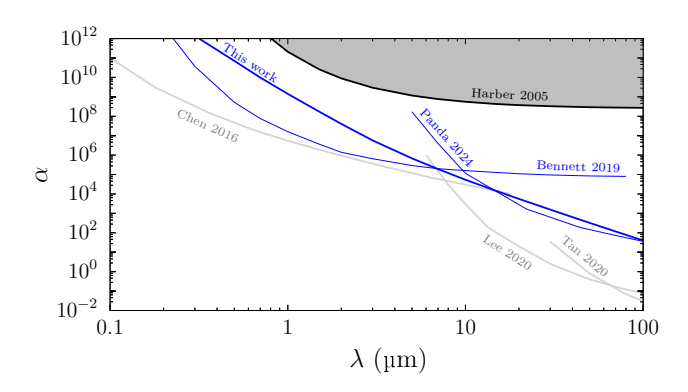


FIG. 5. (Color online) Constraints on the Yukawa  $\alpha$  and  $\lambda$  parameters from existing atomic (black), existing macroscopic (gray) and proposed atomic (blue) measurements. The Harber 2005 results [21] are measurements based on the oscillation frequency of atoms trapped near a surface. The Bennett 2019 [26] curve is based on a proposed experiment using Bloch oscillations of trapped atoms near a surface. The Panda 2024 [20] curve is based on a proposed measurement using a lattice-based interferometer near a surface. The Chen 2016 [10], Lee 2020 [11] and Tan 2020 [12] curves are measurements using torsion pendula.

width of the condensate, meaning that the fringes can still be observed using an imaging beam that travels at a small angle relative to the surface and subsequently reflects off of the membrane, avoiding the membrane edges. A similar method was used by Harber *et al.* to image atoms as close as 6 µm to a surface. This method would produce two images of the atoms, one direct and one reflected. The center of symmetry of the combined image could be used to determine the location of the membrane itself and provide a phase reference.

The sensitivity of the interferometer will depend on how accurately the fringe phase can be determined, which is likely to be limited by the interaction noise described above. We suppose here that the atom number can be measured with 1% accuracy, corresponding to phase noise of 0.1 rad. By averaging on the order of  $10^4$  measurements, the sensitivity can be reduced to about 1 mrad, which we take as a practical limit. Assuming an experimental rate of 250 runs per day, this could be achieved in a two-month measurement campaign.

The sensitivity also depends on the incident velocity  $v_0$ , which can be controlled through the initial confinement strength of the atom trap along x and the timing of the imaging pulse. Larger velocities can be obtained by releasing the atoms from a moving trap. The optimum sensitivity for a given  $\lambda$  occurs at  $v_{\rm opt} = (\beta^2/\lambda^2)v_c$ , but achieving this is limited on the low side by accessible atom energies, and on the high side by the critical velocity for quantum reflection. We suppose that velocities in the range of 50  $\mu$ m/s to 1 mm/s can be accessed and provide sufficient reflection for measurement.

With these assumptions, we achieve the sensitivity lim-

its shown in Fig. 5. Here the black curve and gray shading indicate existing limits for microscopic particles. The heavy blue curve shows our result, and the lighter blue curves are for two other proposed microscopic measurements. The gray curves show existing limits for macroscopic measurements. Given the assumption of a mass-dependent force, it is difficult for atomic measurements to reach the sensitivity of a macroscopic object. However, the method proposed here would improve on existing atomic limits by several orders of magnitude, which would provide a useful constraint on chameleon-style theories with short-range interactions.

At lower  $\lambda$  values, the sensitivity determined here is comparable to that obtained by Bennett and O'Dell [26], but potentially easier to implement experimentally since a high-precision Bloch oscillation frequency measurement is not required. At higher- $\lambda$  values, our approach is competitive with proposed improvements to an optical-lattice interferometer experiment by Panda et~al.~[20], but may again be easier to implement.

### V. CONCLUSIONS

Our results illustrate the possibility of using a quantum reflection interferometer to probe surface effects. Applied, as here, to searching for an anomalous short-range force, we find that the method is promising for improving existing limits on coupling to microscopic bodies like atoms.

The method could more broadly be applied to the measurement of ordinary atom-surface interactions, such as electrostatic patch potentials or the Casimir-Polder force itself. Absolute measurements may be challenging due to the significant phase contribution from atomic interactions, but in many cases differential measurements are still useful. For instance, it should be possible to measure the temperature dependence of the Casimir-Polder force by varying the temperature of the surface [43], or to investigate slow temporal variations in patch potential effects [44]. Alternatively, using a Feshbach measurement to suppress interactions might allow for precision measurements of the  $C_4$  coefficient.

Applications such as these are likely to benefit from the fact that the simple analytical model presented here agrees well with numerical calculations. The model can be readily adapted to other forms for the perturbation V.

Interferometric methods such as this are most easily analyzed in terms of potential energies rather than forces, but it is nonetheless interesting to evaluate the force sensitivity implied by our results. For the conditions of Fig. 2, the nominal reflection distance is  $x_0 \approx 2.3$  µm, at which point the strength of the Yukawa force -dV/dx is quite small,  $1.5 \times 10^{-28}$  N. As seen in the figure, this force yields a distinguishable phase shift in a single measurement. The interaction time with the surface can be estimated as  $\lambda/v_0 \approx 75$  ms, using  $v_0 \approx 0.2$  mm/s. This

illustrates that the method can provide high force sensitivity in a small volume and short time, which could be useful for a variety of applications.

### ACKNOWLEDGMENTS

The authors gratefully acknowledge advice from Mark Edwards regarding solving the GP equation, and comments on the manuscript from Christian Brandt, Zekun Chu, and Itzal De Urioste Terrazas. This work was supported by the National Science Foundation, Grant No. 2110471. J.R.B. is supported by the NSF Graduate Research Fellowship Program under Grant No. DGE 2137420.

- N. Arkani-Hamed, S. Dimopoulos, and G. Dvali, Phys. Rev. D 59, 086004 (1999).
- [2] E. G. Adelberger, B. R. Heckel, and A. E. Nelson, Annu. Rev. Nucl. Part. Sci. 53, 77 (2003).
- [3] J. E. Moody and F. Wilczek, Phys. Rev. D 30, 130 (1984).
- [4] J. A. Frieman, C. T. Hill, A. Stebbins, and I. Waga, Phys. Rev. Lett. 75, 2077 (1995).
- [5] L. J. Hall, Y. Nomura, and S. J. Oliver, Phys. Rev. Lett. 95, 141302 (2005).
- [6] J. Khoury and A. Weltman, Phys. Rev. Lett. 93, 171104 (2004).
- [7] D. F. Mota and D. J. Shaw, Phys. Rev. Lett. 97, 151102 (2006).
- [8] J. C. Long and J. C. Price, C. R. Physique 4, 337 (2003).
- [9] A. A. Geraci, S. J. Smullin, D. M. Weld, J. Chiaverini, and A. Kapitulnik, Phys. Rev. D 78, 022002 (2008).
- [10] Y.-J. Chen, W. Tham, D. Krause, D. López, E. Fischbach, and R. Decca, Phys. Rev. Lett. 116, 221102 (2016).
- [11] J. Lee, E. Adelberger, T. Cook, S. Fleischer, and B. Heckel, Phys. Rev.Lett. 124, 101101 (2020).
- [12] W.-H. Tan, A.-B. Du, W.-C. Dong, S.-Q. Yang, C.-G. Shao, S.-G. Guan, Q.-L. Wang, B.-F. Zhan, P.-S. Luo, L.-C. Tu, and J. Luo, Phys. Rev. Lett. 124, 051301 (2020).
- [13] I. Antoniadis, S. Baessler, M. Büchner, V. Fedorov, S. Hoedl, A. Lambrecht, V. Nesvizhevsky, G. Pignol, K. Protasov, S. Reynaud, and Y. Sobolev, C. R. Physique 12, 755 (2011).
- [14] G. Raffelt, Phys. Rev. D 86, 015001 (2012).
- [15] D. F. Jackson Kimball, D. Budker, T. E. Chupp, A. A. Geraci, S. Kolkowitz, J. T. Singh, and A. O. Sushkov, Phys. Rev. A 108, 010101 (2023).
- [16] C. Burrage, E. J. Copeland, and E. Hinds, J. Cosmol. Astropart. Phys 2015, 042 (2015).
- [17] P. Hamilton, M. Jaffe, P. Haslinger, Q. Simmons, H. Müller, and J. Khoury, Science 349, 849 (2015).
- [18] S. Schlögel, S. Clesse, and A. Füzfa, Phys. Rev. D 93, 104036 (2016).
- [19] M. Jaffe, P. Haslinger, V. Xu, P. Hamilton, A. Upadhye, B. Elder, J. Khoury, and H. Müller, Nature Phys. 13, 938 (2017).
- [20] C. D. Panda, M. J. Tao, M. Ceja, J. Khoury, G. M. Tino, and H. Müller, Nature 631, 515 (2024).
- [21] D. Harber, J. Obrecht, J. McGuirk, and E. Cornell, Phys. Rev. A 72, 033610 (2005).
- [22] F. Shimizu, Phys. Rev. Lett. **86**, 987 (2001).
- [23] A. Mody, M. Haggerty, J. M. Doyle, and E. J. Heller, Phys. Rev. B 64, 085418 (2001).

- [24] T. A. Pasquini, Y. Shin, C. Sanner, M. Saba, A. Schirotzek, D. E. Pritchard, and W. Ketterle, Phys. Rev. Lett. 93, 223201 (2004).
- [25] T. A. Pasquini, M. Saba, G. Jo, Y. Shin, W. Ketterle, D. E. Pritchard, T. A. Savas, and N. Mulders, Phys. Rev. Lett. 97, 260402 (2006).
- [26] R. Bennett and D. H. J. O'Dell, New J. Phys. 21, 033032 (2019).
- [27] H. B. G. Casimir and P. Polder, Phys. Rev. 73, 360 (1948).
- [28] C. Carraro and M. W. Cole, Prog. Surf. Sci. 57, 61 (1998).
- [29] H. Friedrich and A. Jurisch, Phys. Rev. Lett. 92, 103202 (2004).
- [30] E. Floratos and G. Leontaris, Phys. Lett. B 465, 95 (1999).
- [31] A. D. Cronin, J. Schmiedmayer, and D. E. Pritchard, Rev. Mod. Phys. 81, 1051 (2009).
- [32] A. Shih and V. A. Parsegian, Phys. Rev. A 12, 835 (1975).
- [33] A. Derevianko and W. R. Johnson, Phys. Rev. A 57, 2629 (1998).
- [34] T. Kovachy, P. Asenbaum, C. Overstreet, C. A. Donnelly, S. M. Dickerson, A. Sugarbaker, J. M. Hogan, and M. A. Kasevich, Nature 528, 530 (2015).
- [35] N. Gaaloul, M. Meister, R. Corgier, A. Pichery, P. Boegel, W. Herr, H. Ahlers, E. Charron, J. R. Williams, R. J. Thompson, W. P. Schleich, E. M. Rasel, and N. P. Bigelow, Nature Commun. 13, 10.1038/s41467-022-35274-6 (2022).
- [36] X. Antoine, A. Arnold, C. Besse, M. Ehrhardt, and A. Schädle, Comm. Comp. Phys. 4, 729 (2008).
- [37] E. Galiffi, C. Sünderhauf, M. DeKieviet, and S. Wimberger, Journal of Physics B: Atomic, Molecular and Optical Physics 50, 095001 (2017).
- [38] F. Dalfovo, S. Giorgini, L. Pitaevskii, and S. Stringari, Rev. Mod. Phys. 71, 463 (1999).
- [39] W. Bao, D. Jaksch, and P. A. Markowich, J. Comp. Phys. 187, 318 (2003).
- [40] A. A. Geraci, S. B. Papp, and J. Kitching, Phys. Rev. Lett. 105, 101101 (2010).
- [41] J. R. Dwyer and M. Harb, Appl. Spectrosc. 71, 2051 (2017).
- [42] T. Tanimura, T. Kashiwaya, S. Tange, Y. Tanaka, H. Iida, T. Yoshioka, K. Masuda, and T. Ryu, in *Inter-national Conference on Extreme Ultraviolet Lithography* 2024, edited by J.-H. Franke, K. G. Ronse, P. A. Gargini, P. P. Naulleau, and T. Itani (SPIE, 2024) p. 24.
- [43] J. Obrecht, R. Wild, M. Antezza, L. Pitaevskii,

S. Stringari, and E. Cornell, Phys. Rev. Lett.  $\bf 98,\,063201$  (2007).

[44] H. Yin, Y.-Z. Bai, M. Hu, L. Liu, J. Luo, D.-Y. Tan, H.-C. Yeh, and Z.-B. Zhou, Phys. Rev. D 90, 122001 (2014).